

## Elastic Plastic and Damage Model for Concrete Materials: Part II: Implementation and Application to Concrete and Reinforced Concrete

Ziad N. Taqieddin\* and George Z.Voyiadjis

*Department of Civil Engineering, Applied Science University, Amman, Jordan*

### Abstract:

In this companion article, we present, within the finite element context, the numerical algorithms for the integration of the thermodynamically consistent formulation of the elastic plastic and damage model for concrete materials derived in part I of this work. The proposed unified integration scheme is based on the spectral return-mapping algorithm accounting for the use of the principal stresses along with the stress tensor invariants. An operator split structure is used, consisting of a trial stress state followed by corrector steps applied through imposing the generalized plastic and damage consistency conditions. Furthermore, a trivially incrementally objective integration scheme is established for the rate constitutive relations. The proposed elastic-predictor and uncoupled plastic and damage corrector algorithms allow for a straightforward integration scheme that can be easily implemented into the existing finite element codes. The nonlinear algebraic system of equations is solved by consistent linearization and the Newton–Raphson iteration scheme. The proposed model is implemented in the implicit finite element code ABAQUS via the user subroutine UMAT. Model capabilities are illustrated through its application to the analysis of Reinforced Concrete (RC) beams tested experimentally and available in literature. The simulated results illustrate the potential of the proposed model in dealing with the reduction of the effect of the well known mesh sensitivity problem through the application of the fracture energy concept-related parameters.

**Keywords:** Nonlinear Finite Elements, Implicit/Explicit Integration, Operator split Structured algorithm, Reinforced Concrete.

### 1. Introduction

Capturing the softening behavior of quasi-brittle materials in general and concrete in particular is an important issue when dealing with the constitutive modeling of such materials. Localization due to softening and the accompanying reduction in strength are prevalent characteristic behaviors that need to be addressed for a constitutive model to successfully describe the mechanical behavior of concrete. The application of continuum damage mechanics combined to concrete elasto-plasticity theory sets forth the theoretical background for deriving such appropriate concrete constitutive models (e.g. Mazars and Pijaudier-Cabot, 1989; Yazdani and Schreyer, 1990; Lee and Fenves, 1998, 2001; Faria et. al., 1998; Fichant et. al., 1999; Nechnech et. al., 2002; Willam et. al., 2003; Jefferson, 2003; Salari et. al., 2004; Shen et. al., 2004; Tashman et. al., 2005; Jason et. al., 2006; Contrafatto and Cuomo, 2006; Cicekli et. al., 2007; Voyiadjis et. al., 2008a,b; Červenka and Papanikolaou, 2008; and Taqieddin, 2008).

This article establishes and discusses the integration procedure and numerical aspects related to the elastic-plastic and damage model presented in part I of this work. The numerical implementation of any constitutive model is just as important as the constitutive model itself. A brief literature review can reveal several mathematically elegant models that are extremely hard to implement or to achieve convergence. Therefore, a constitutive model should be rigorously derived based on sound thermodynamic principles, yet simple and robust when implemented into FE codes.

The spectral return-mapping algorithm suggested by Simo (1992) and later used by Lee and Fenves (2001) and Wu et. al. (2006) is adopted here. This algorithm is based on the principal stress space and employs the spectral decomposition of the trial stress to decouple the return-mapping algorithm. The operator split concept is used, where the incremental constitutive equation is decomposed into elastic, plastic and damage parts, leading to the corresponding numerical elastic-predictor, plastic-corrector and damage-corrector steps.

In part I of this work (Voyiadjis et. al, 2008c), an elastic plastic damage formulation is proposed to model the nonlinear behavior of concrete materials. The model is intended to circumvent the disadvantages of pure plastic and pure damage approaches applied separately. It is based on an isotropic damage model, with tensile and compressive

\*Email: z\_taqieddin@asu.edu.jo

damage criteria, combined to an effective stress space plasticity yield criterion with multiple hardening rules. The isotropic damage is responsible for the softening response and the decrease in the elastic stiffness, while hardening plasticity accounts for the development of irreversible strains and volumetric compressive behavior within the effective configuration. Fracture energy related coefficients have been defined and incorporated in order to achieve a reasonable degree of discretization insensitivity in numerical calculations.

The effective stress space plasticity is combined with continuum damage mechanics to provide a simple way to separate the damage and plastic processes in the numerical scheme. Plastic effects, driven by the effective stresses, can be described independently from damage ones and vice versa, in order to ease the numerical implementation which is Implicit/Explicit. The plastic part is Implicit and the damage part is Explicit, same as in classical continuum damage computations. As a consequence, the above mentioned robust algorithm for integrating the constitutive relations can be implemented. The calibration of the material parameters is also easier to handle as a consequence of the separation of damage and plasticity processes. Further details of the theoretical part of this model are presented in Taqieiddin (2008). The key ingredients of the constitutive model are summarized in Table 1, representing the theoretical background upon which the integration scheme is based.

The proposed model, along with its implementation algorithm, is then applied to study RC beams. In this study, the two dimensional RC beam analysis will consist of three major components: steel reinforcing bars, concrete material, and bond effect. Steel reinforcing bars will be modeled using the discrete representation in the FE mesh. The reinforcing steel elastoplastic material model is described in Taqieiddin (2008), and will be used here with linear strain hardening. The concrete behavior will be described using the elastic-plastic-damage model discussed in part I of this work. The overall effect of bond deterioration and the transfer of the stresses from concrete to the reinforcing bars will be accounted for using the work of Belarbi and Hsu (1994) which was modified later on by Kwak and Kim (2006). The bond-slip effect along the reinforcing bars is quantified with the force equilibrium and compatibility condition at the post-cracking stage and its contribution is indirectly implemented into the stress-strain relation of reinforcing steel. The advantage of the analytical procedures proposed by Belarbi and Hsu (1994) and Kwak and Kim (2006) is taking into account the incorporation of the bond slip effect while using the conventional discrete representation of steel, without the need for additional considerations such as using double nodes or interface elements.

In the following sections, the numerical integration scheme of the constitutive model is derived. The elastic predictor, plastic corrector steps and presented with the effective stress space framework, followed by the damage corrector which transforms the effective stress into the actual (damaged) configuration. Examples of RC beams tested experimentally by different researchers and available in literature are studied and discussed.

## 2. Numerical Integration of the Constitutive Model

Let  $t_0, t_1, t_2, \dots, t_n, t_{n+1} = t_n + \Delta t, \dots$ , be convenient time instances along the time interval over which the material's response of the structure is sought. Considering the time step  $\Delta t = t_{n+1} - t_n$  starting at  $t = t_n$  where all quantities are known, i.e. converged values of the previous step, the solution must be computed at  $t_{n+1}$  for a given load increment. The state variables are to be updated to the new configuration according to the additive decomposition where  $(\cdot)_{n+1} = (\cdot)_n + \Delta(\cdot)$ . The general 3D formulation will be provided here for thoroughness and the 2D cases can be easily obtained by considering the number of contributing stresses.

The development of a computational algorithm that is consistent with the proposed theoretical formulation is given in details in this section to facilitate the numerical integration of the constitutive equations in the context of the FE method. According to the operator split concept of (Ju, 1989; Simo and Hughes, 1998), the rate form of the constitutive equation, Eq. (2), can be decomposed into elastic, plastic and damage parts, leading to the corresponding numerical algorithm including elastic-predictor, plastic-corrector and damage-corrector steps (Lee and Fenves, 2001; Wu et. al., 2006, Jason et. al., 2006) as follows:

$$\begin{aligned} \dot{\sigma}_{ij} &= (1 - \Phi) \dot{\bar{\sigma}}_{ij} - \dot{\Phi} \bar{\sigma}_{ij} \\ \Delta \sigma_{ij} &= (1 - \Phi) (\bar{E}_{ijkl} \Delta \varepsilon_{kl} - \bar{E}_{ijkl} \Delta \varepsilon_{kl}^p) - \Delta \Phi \bar{E}_{ijkl} \varepsilon_{kl}^e \\ \Delta \sigma_{ij} &= (1 - \Phi) \left( \underbrace{\Delta \bar{\sigma}_{ij}^{trial}}_{\text{ELASTIC PREDICTOR}} - \underbrace{\bar{E}_{ijkl} \Delta \varepsilon_{kl}^p}_{\text{PLASTIC CORRECTOR}} \right) - \Delta \Phi \bar{E}_{ijkl} \varepsilon_{kl}^e \end{aligned} \quad (1)$$

In the first step, the elastic-predictor problem is solved with the initial conditions being the converged values of the previous iteration ( $t = t_n$ ) along with the new increment while keeping the irreversible variables frozen. This produces a trial stress state,  $\bar{\sigma}_{ij}^{trial} = \bar{\sigma}_{ij}^n + \Delta \bar{\sigma}_{ij}^{trial}$ , which, if outside the plastic surface  $f$  and the damage surfaces  $g^\pm$

Table 1. Constitutive Model

## 1. Relationship between stresses in the effective and damaged configuration

$$\sigma_{ij} = (1 - \Phi) \bar{\sigma}_{ij} = (1 - \Phi) \bar{E}_{ijkl} \varepsilon_{kl}^e = (1 - \Phi) \bar{E}_{ijkl} (\varepsilon_{kl} - \varepsilon_{kl}^p) \quad (2)$$

$$\bar{E}_{ijkl} = 2\bar{G}I_{ijkl}^{dev} + \bar{K}\delta_{ij}\delta_{kl} \quad , \quad \Phi = \frac{\left[ \left[ \bar{\sigma}_{ij}^+ \right] \varphi^+ + \left[ \bar{\sigma}_{ij}^- \right] \varphi^- \right]}{\left[ \left[ \bar{\sigma}_{ij} \right] \right]} \quad (3)a,b$$

## 2. Effective stress space plasticity yield criterion, hardening rules and variables

$$f = \sqrt{3\bar{J}_2} + \alpha \bar{I}_1 + \beta (\kappa^\pm) H(\hat{\sigma}_{\max}^\pm) \hat{\sigma}_{\max}^\pm - (1 - \alpha) c^-(\kappa^-) = 0 \quad (4)$$

$$c^+(\kappa^+) = f_0^+ + h \kappa^+ \quad , \quad c^-(\kappa^-) = f_0^- + Q \left[ 1 - \exp(-\omega \kappa^-) \right] \quad (5)a,b$$

$$\dot{\kappa}^+ = r(\hat{\sigma}_i^\pm) \hat{\varepsilon}_{\max}^p \quad , \quad \dot{\kappa}^- = -(1 - r(\hat{\sigma}_i^\pm)) \hat{\varepsilon}_{\min}^p \quad (6)a,b$$

$$\dot{c}^+ = h \dot{\kappa}^+ \quad , \quad \dot{c}^- = \omega(Q - c_i^-) \dot{\kappa}^- \quad (7)a,b$$

## 3. Damage criteria, hardening rules, and thermodynamic conjugate forces

$$g^\pm = Y^\pm - Y_0^\pm - Z^\pm \leq 0 \quad , \quad Z^\pm = \frac{1}{a^\pm} \left( \frac{\varphi^\pm}{1 - \varphi^\pm} \right)^{\frac{1}{b^\pm}} \quad , \quad \chi = 1 - \frac{1}{1 + cY \exp(-dY)} \quad (8)a-c$$

$$Y^\pm = -\rho \frac{\partial \psi^e}{\partial \varphi^\pm} = \frac{1}{2} \frac{\left\| \bar{\sigma}_{ij}^\pm \right\|}{\left\| \bar{\sigma}_{ij} \right\|} \left( \varepsilon_{ij}^e \bar{E}_{ijkl} \varepsilon_{kl}^e - \frac{1}{9} (1 - \chi^\pm) (\varepsilon_{mm}^e)^2 \delta_{ij} \bar{E}_{ijkl} \delta_{kl} \right) \quad (9)$$

## 4. Effective stress space plasticity flow rule and plastic potential function

$$\dot{\varepsilon}_{ij}^p = \dot{\lambda} \frac{\partial F^p}{\partial \bar{\sigma}_{ij}} \quad , \quad F^p = \sqrt{3\bar{J}_2} + \alpha^p \bar{I}_1 \quad , \quad \frac{\partial F^p}{\partial \bar{\sigma}_{ij}} = \frac{3}{2} \frac{\bar{s}_{ij}}{\sqrt{3\bar{J}_2}} + \alpha^p \delta_{ij} \quad (10)a-c$$

## 5. Generalized plastic and damage Kuhn-Tucker consistency conditions

**Plastic**

$$f \leq 0, \quad \dot{\lambda}^p \geq 0, \quad \dot{\lambda}^p f = 0$$

$$\text{If } f < 0 \rightarrow \dot{\lambda}^p = 0, \quad \text{if } f = 0 \rightarrow \dot{\lambda}^p \dot{f} = 0 \quad (11)$$

$$\text{If } f = 0 \text{ and } \dot{f} < 0 \text{ then } \dot{\lambda}^p = 0$$

$$\text{If } f = 0 \text{ and } \dot{f} = 0 \text{ then } \dot{\lambda}^p > 0$$

**Damage**

$$\text{If } g^\pm < 0 \quad \text{then } \dot{\varphi}^\pm = 0$$

$$\text{If } g^\pm = 0 \text{ and } \dot{g}^\pm < 0 \quad \text{then } \dot{\varphi}^\pm = 0 \quad (12)$$

$$\text{If } g^\pm = 0 \text{ and } \dot{g}^\pm = 0 \quad \text{then } \dot{\varphi}^\pm > 0$$

## 6. Elastic/Damage and Plastic parts of the Helmholtz Free Energy (HFE) Function

$$\rho \psi^e = \frac{1}{2} (1 - \Phi) \varepsilon_{ij}^e \bar{E}_{ijkl} \varepsilon_{kl}^e + \frac{1}{2} (1 - \chi) \Phi \left( \frac{1}{9} (\varepsilon_{mm}^e)^2 \delta_{ij} \bar{E}_{ijkl} \delta_{kl} \right) \quad (13)$$

$$\rho \psi^p = f_0^+ \kappa^+ + \frac{1}{2} h (\kappa^+)^2 + f_0^- \kappa^- + Q \left( \kappa^- + \frac{1}{\omega} \exp(-\omega \kappa^-) \right) \quad (14)$$

is taken as the initial conditions for the solution of the plastic-corrector and damage-corrector problems. The scope of the second and third steps is to restore the generalized plasticity and damage consistency conditions by returning back the trial stress to the plastic surface  $f$  and the damage surfaces  $g^\pm$ .

During the elastic-predictor  $\Delta \bar{\sigma}_{ij}^{trial}$  and the plastic-corrector  $-\bar{E}_{ijkl} \Delta \varepsilon_{kl}^p$  steps the damage variables are fixed, so that the elastic-plastic behavior is decoupled from damage, constituting a standard elastic-plastic problem in the effective stress space. Regarding the adopted plastic yield function, Eq.(4), the spectral decomposition form (Lee and Fenves, 2001) of return-mapping algorithm (Simo and Hughes, 1998) is applied to update the effective stress tensor  $\bar{\sigma}_{ij}^{n+1}$ . Once the effective stress tensor  $\bar{\sigma}_{ij}^{n+1}$  is updated in the elastic-predictor and plastic-corrector steps, the damage variables  $(\varphi^\pm)^{n+1}$  (and therefore  $\Phi^{n+1}$ ) and the Cauchy stress tensor  $\sigma_{ij}^{n+1}$  can then be updated correspondingly in the damage-corrector step (Wu et. al., 2006).

The (degradation) damage-corrector is implemented separately from the plastic-corrector part because  $(\varphi^\pm)^{n+1}$  (and therefore  $\Phi^{n+1}$ ) are functions of the updated effective stress tensor  $\bar{\sigma}_{ij}^{n+1}$  and its corresponding elastic strain tensor  $(\varepsilon_{kl}^e)^{n+1} = (\varepsilon_{kl}^e)^n + \Delta \varepsilon_{kl}^e$ , which are completely determined during the plastic-corrector step  $\Delta \varepsilon_{kl}^e = \Delta \varepsilon_{kl} - \Delta \varepsilon_{kl}^p$ .

A fully Implicit (Backward-Euler) scheme is used for the stress computation problem in the effective space, followed by an explicit integration scheme for the updated damage variables and Cauchy stress tensor. The integration procedure start at the beginning of the  $(n, n+1)$  step where  $\bar{\sigma}_{ij}^n, (\varepsilon_{ij}^p)^n, (\kappa^\pm)^n$  (adopted here for simplicity as  $\kappa^n$ ) and  $\Delta \varepsilon_{ij}$  are all known from the previous step  $(n-1, n)$ .

### 2.1. The Effective (Undamaged) Elastic-Plastic Steps

In this section, the elastic-plastic integration procedure is carried out in an undamaged medium. Therefore, the stresses and strains will carry a superimposed dash indicating the effective configuration. The ultimate goal of the elastic-plastic steps is to update the effective stress tensor and the hardening parameters. The updated effective stress is given as:

$$\begin{aligned} \bar{\sigma}_{ij}^{n+1} &= \bar{E}_{ijkl} (\bar{\varepsilon}_{kl}^e)^{n+1} = \bar{E}_{ijkl} (\bar{\varepsilon}_{kl}^{n+1} - (\bar{\varepsilon}_{kl}^p)^{n+1}) = \bar{E}_{ijkl} (\bar{\varepsilon}_{kl}^n + \Delta \bar{\varepsilon}_{kl} - (\bar{\varepsilon}_{kl}^p)^n - \Delta \bar{\varepsilon}_{kl}^p) \\ &= \bar{E}_{ijkl} (\bar{\varepsilon}_{kl}^n - (\bar{\varepsilon}_{kl}^p)^n) + \bar{E}_{ijkl} (\Delta \bar{\varepsilon}_{kl} - \Delta \bar{\varepsilon}_{kl}^p) = \bar{E}_{ijkl} (\bar{\varepsilon}_{kl}^e)^n + \bar{E}_{ijkl} \Delta \bar{\varepsilon}_{kl}^e \\ &= \bar{\sigma}_{ij}^n + \Delta \bar{\sigma}_{ij} \end{aligned} \quad (15)$$

#### 2.1.1. The Elastic - Predictor

The elastic predictor problem defines the stress in the trial state assuming an entirely elastic strain increment ( $\Delta \bar{\varepsilon}_{ij} = \Delta \bar{\varepsilon}_{ij}^e$ ) as:

$$\begin{aligned} \bar{\sigma}_{ij}^{trial} &= \bar{E}_{ijkl} (\bar{\varepsilon}_{kl}^{n+1} - (\bar{\varepsilon}_{kl}^p)^n) = \bar{E}_{ijkl} (\bar{\varepsilon}_{kl}^n + \Delta \bar{\varepsilon}_{kl} - (\bar{\varepsilon}_{kl}^p)^n) \\ &= \bar{E}_{ijkl} (\bar{\varepsilon}_{kl}^n - (\bar{\varepsilon}_{kl}^p)^n) + \bar{E}_{ijkl} \Delta \bar{\varepsilon}_{kl} = \bar{E}_{ijkl} (\bar{\varepsilon}_{kl}^e)^n + \bar{E}_{ijkl} \Delta \bar{\varepsilon}_{kl} \\ &= \bar{\sigma}_{ij}^n + \bar{E}_{ijkl} \Delta \bar{\varepsilon}_{kl} = \bar{\sigma}_{ij}^n + \Delta \bar{\sigma}_{ij}^{trial} \end{aligned} \quad (16)$$

where  $\bar{\sigma}_{ij}^n$  is calculated in the previous  $(n)$  step.

In order to verify the correctness of this elastic prediction, the trial stress is applied into the yield function  $f(\bar{\sigma}_{ij}^{trial}, \kappa^n)$ . If  $f(\bar{\sigma}_{ij}^{trial}, \kappa^n) < 0$ , the process is elastic and the trial state is admissible and accepted as the final state since there is no change in the plastic strain, such that:

$$\bar{\sigma}_{ij}^{n+1} = \bar{\sigma}_{ij}^{trial}, \quad (\bar{\varepsilon}_{ij}^p)^{n+1} = (\bar{\varepsilon}_{ij}^p)^n, \quad (\kappa^\pm)^{n+1} = (\kappa^\pm)^n \quad (17)$$

On the other hand, if  $f(\bar{\sigma}_{ij}^{trial}, \kappa^n) > 0$ , the Kuhn-Tucker loading/unloading conditions are violated by the trial state which now lies outside the yield surface. Then the consistency is resorted by the return-mapping/plastic-corrector step.

### 2.1.2. The Plastic – Corrector

If the current step is not an elastic state,  $f(\bar{\sigma}_{ij}^{trial}, \kappa^n) > 0$ , the plastic strain tensor will change. To compute the effective stress along with the plastic strain tensor at the current time increment requires iterations within that time increments for the effective stress in the plastic-corrector step. During these iterations, the discrete version of the plastic consistency condition is imposed as a constraint,  $f(\bar{\sigma}_{ij}^{n+1}, \kappa^{n+1}) = 0$ , at the end of each iteration. Therefore, the analysis is transformed into a linear set of equations that depend on the material parameters and on the current coordinates of the integration points within each iteration. The outcomes of the plastic-corrector step are the updated effective stress tensor  $\bar{\sigma}_{ij}^{n+1}$ , plastic strain tensor  $(\bar{\varepsilon}_{ij}^p)^{n+1}$ , and plastic variables  $(\kappa^\pm)^{n+1}$ . The plastic-corrector step can be derived as follows:

$$\begin{aligned}\bar{\sigma}_{ij}^{n+1} &= \bar{\sigma}_{ij}^n + \Delta \bar{\sigma}_{ij} = \bar{\sigma}_{ij}^n + \bar{E}_{ijkl} \Delta \bar{\varepsilon}_{kl}^e = (\bar{\sigma}_{ij}^n + \bar{E}_{ijkl} \Delta \bar{\varepsilon}_{kl}^e) - \bar{E}_{ijkl} \Delta \bar{\varepsilon}_{kl}^p \\ &= \bar{\sigma}_{ij}^{trial} - \bar{E}_{ijkl} \Delta \bar{\varepsilon}_{kl}^p\end{aligned}\quad (18)$$

Within the plastic-corrector step, and in order to compute  $\Delta \bar{\varepsilon}_{kl}^p$  in Eq. (18), the radial-return method is used. The flow rule in Eq. (10)a can be written implicitly for the  $(n+1)$  step as follows:

$$\Delta \bar{\varepsilon}_{kl}^p = \Delta \lambda^p \frac{\partial F^p}{\partial \bar{\sigma}_{kl}^{n+1}} \quad (19)$$

where  $\frac{\partial F^p}{\partial \bar{\sigma}_{kl}^{n+1}}$  (Eq. (10)c) is given here as the following:

$$\frac{\partial F^p}{\partial \bar{\sigma}_{kl}^{n+1}} = \sqrt{\frac{3}{2}} \frac{\bar{S}_{kl}^{n+1}}{\|\bar{S}_{mn}^{n+1}\|} + \alpha_p \delta_{kl} \quad (20)$$

where  $\|\bar{S}_{mn}^{n+1}\| = \sqrt{\bar{S}_{mn}^{n+1} \bar{S}_{mn}^{n+1}}$  is the norm of the updated effective deviatoric stresses.

By substituting the elasticity tensor in the undamaged configuration,  $\bar{E}_{ijkl}$  (Eq.(3)a), into Eq. (18), the effective stress can be updated using the return-mapping equation given as follows (see Taqueiddin (2008)):

$$\bar{\sigma}_{ij}^{n+1} = \bar{\sigma}_{ij}^{trial} - \left[ 2\bar{G} \Delta \bar{\varepsilon}_{ij}^p + \left( \bar{K} - \frac{2}{3} \bar{G} \right) \Delta \bar{\varepsilon}_{kk}^p \delta_{ij} \right] \quad (21)$$

where  $\Delta \bar{\varepsilon}_{kk}^p$  can now be obtained from Eqs. (19) and (20) as follows:

$$\Delta \bar{\varepsilon}_{kk}^p = 3\alpha_p \Delta \lambda^p \quad (22)$$

By substituting Eqs. (19), (20), and (22) into Eq.(21) one obtains:

$$\bar{\sigma}_{ij}^{n+1} = \bar{\sigma}_{ij}^{trial} - \left[ 2\bar{G} \Delta \lambda^p \left\{ \sqrt{\frac{3}{2}} \frac{\bar{S}_{ij}^{n+1}}{\|\bar{S}_{mn}^{n+1}\|} + \alpha_p \delta_{ij} \right\} + \left( \bar{K} - \frac{2}{3} \bar{G} \right) (3\alpha_p \Delta \lambda^p) \delta_{ij} \right] \quad (23)$$

Expanding and then simplifying the above equation, one can obtain the following form:

$$\begin{aligned}\bar{\sigma}_{ij}^{n+1} &= \bar{\sigma}_{ij}^{trial} - \left[ \sqrt{6} \bar{G} \Delta \lambda^p \frac{\bar{S}_{ij}^{n+1}}{\|\bar{S}_{mn}^{n+1}\|} + 2\bar{G} \alpha_p \Delta \lambda^p \delta_{ij} + 3\bar{K} \alpha_p \Delta \lambda^p \delta_{ij} - 2\bar{G} \alpha_p \Delta \lambda^p \delta_{ij} \right] \\ &\bar{\sigma}_{ij}^{n+1} = \bar{\sigma}_{ij}^{trial} - \Delta \lambda^p \left[ \sqrt{6} \bar{G} \frac{\bar{S}_{ij}^{n+1}}{\|\bar{S}_{mn}^{n+1}\|} + 3\bar{K} \alpha_p \delta_{ij} \right]\end{aligned}\quad (24)$$

Separating Eq. (24) into deviatoric and volumetric parts gives the following:

$$\begin{aligned}
I_{ijkl}^{dev} \bar{\sigma}_{kl}^{n+1} &= I_{ijkl}^{dev} \bar{\sigma}_{kl}^{trial} - \Delta\lambda^p I_{ijkl}^{dev} \left[ \sqrt{6\bar{G}} \frac{\bar{S}_{kl}^{n+1}}{\|\bar{S}_{mn}^{n+1}\|} + 3\bar{K}\alpha_p \delta_{kl} \right] \\
\bar{S}_{ij}^{n+1} &= \bar{S}_{ij}^{trial} - \Delta\lambda^p \left( \frac{1}{2} (\delta_{ik} \delta_{jl} + \delta_{il} \delta_{jk}) - \frac{1}{3} \delta_{ij} \delta_{kl} \right) \left[ \sqrt{6\bar{G}} \frac{\bar{S}_{kl}^{n+1}}{\|\bar{S}_{mn}^{n+1}\|} + 3\bar{K}\alpha_p \delta_{kl} \right] \\
\bar{S}_{ij}^{n+1} &= \bar{S}_{ij}^{trial} - \sqrt{6\Delta\lambda^p \bar{G}} \frac{\bar{S}_{ij}^{n+1}}{\|\bar{S}_{ij}^{n+1}\|}
\end{aligned} \tag{25}$$

and

$$\begin{aligned}
\bar{\sigma}_{ii}^{n+1} &= \bar{\sigma}_{ii}^{trial} - \Delta\lambda^p \left[ \sqrt{6\bar{G}} \frac{\bar{S}_{ii}^{n+1}}{\|\bar{S}_{mn}^{n+1}\|} + 3\bar{K}\alpha_p \delta_{ii} \right] \\
\bar{I}_1^{n+1} &= \bar{I}_1^{trial} - 9\Delta\lambda^p \bar{K}\alpha_p
\end{aligned} \tag{26}$$

To solve for the plastic multiplier  $\Delta\lambda^p$  from Eq. (25), the radial-return method is applied. The proof of the radial-return applied to Eq. (25) is provided in Taqeiddin (2008) and the result is stated here as:

$$\frac{\bar{S}_{ij}^{n+1}}{\|\bar{S}_{ij}^{n+1}\|} = \frac{\bar{S}_{ij}^{trial}}{\|\bar{S}_{ij}^{trial}\|} \tag{27}$$

Therefore, substituting Eq. (27) into Eq. (25), the radial-return form of Eq. (25) can be provided as follows:

$$\bar{S}_{ij}^{n+1} = \bar{S}_{ij}^{trial} - \sqrt{6\Delta\lambda^p \bar{G}} \frac{\bar{S}_{ij}^{trial}}{\|\bar{S}_{ij}^{trial}\|} \tag{28}$$

and a direct result of the radial return concept is the following equation:

$$\|\bar{S}_{ij}^{n+1}\| = \|\bar{S}_{ij}^{trial}\| - \sqrt{6\bar{G}\Delta\lambda^p} \tag{29}$$

Equation (24) can eventually be written as follows:

$$\bar{\sigma}_{ij}^{n+1} = \bar{\sigma}_{ij}^{trial} - \Delta\lambda^p \left[ \sqrt{6\bar{G}} \frac{\bar{S}_{ij}^{trial}}{\|\bar{S}_{mn}^{trial}\|} + 3\bar{K}\alpha_p \delta_{ij} \right] \tag{30}$$

Next, in order to account for the effective principal stress term in the plasticity yield function, Eq. (4), the spectral return-mapping algorithm of (Simo, 1992; Lee and Fenves, 2001) is used. This algorithm has the advantage for yield function which includes principal stress terms in addition to the stress tensor invariants (Wu et. al., 2006). A decoupled version of the return-mapping algorithm is derived (using the spectral decomposition concept) and shown below.

The spectral decomposition of the stress at step  $n+1$  is given as follows:

$$\bar{\sigma}_{ij}^{n+1} = l_{ir} \hat{\sigma}_{rs}^{n+1} l_{js} \tag{31}$$

where  $l_{mn}$  is the principal direction tensor corresponding to the effective principle stress tensor. Lee and Fenves, (2001), showed that the plastic potential function  $F^p$  can be written in terms of the effective principal stresses such that the increment of the effective plastic strain  $\Delta\bar{\epsilon}_{ij}^p$  can be written as follows:

$$\Delta\bar{\epsilon}_{ij}^p = \Delta\lambda^p l_{ir} \frac{\partial F^p}{\partial \hat{\sigma}_{rs}^{n+1}} l_{js} \tag{32}$$

By substituting Eqs. (22), (31), and (32) into Eq. (21), one can write the return-mapping equation in the following form:

$$l_{ir} \hat{\sigma}_{rs}^{n+1} l_{js} = \bar{\sigma}_{ij}^{trial} - \left[ 2\bar{G} \Delta \lambda^p l_{ir} \frac{\partial F^p}{\partial \hat{\sigma}_{rs}^{(n+1)}} l_{js} + 3(\bar{K} - \frac{2}{3}\bar{G}) \alpha_p \Delta \lambda^p \delta_{ij} \right] \quad (33)$$

Using the following relation for the Kronecker delta, which holds for any direction tensor  $l_{mn}$  :

$$\delta_{ij} = l_{ir} \delta_{rs} l_{js} \quad (34)$$

one can write Eq. (33) in the following form to obtain the effective trial stress directly as:

$$\bar{\sigma}_{ij}^{trial} = l_{ir} \hat{\sigma}_{rs}^{n+1} l_{js} + \Delta \lambda^p l_{ir} \left[ 2\bar{G} \frac{\partial F^p}{\partial \hat{\sigma}_{rs}^{n+1}} + 3(\bar{K} - \frac{2}{3}\bar{G}) \alpha_p \delta_{rs} \right] l_{js} \quad (35)$$

Lee and Fenves (2001) proved that any principal direction tensor for  $\bar{\sigma}_{ij}^{n+1}$  is also a principal direction tensor for  $\bar{\sigma}_{ij}^{trial}$ . This proof is necessary to show that the eigenvector spaces of  $\bar{\sigma}_{ij}^{n+1}$  and  $\bar{\sigma}_{ij}^{trial}$  are exactly identical despite the fact that symmetric tensors do not have a unique spectral decomposition form if they have repeated eigenvalues. Accordingly, the spectral decomposition of the trial stress tensor is given as:

$$\bar{\sigma}_{ij}^{trial} = l_{ir} \hat{\sigma}_{rs}^{trial} l_{js} \quad (36)$$

where  $\hat{\sigma}_{rs}^{trial}$  is the principal trial stress tensor.

From Eq. (35) along with Eq. (36) one can write the decoupled form of the return-mapping equation as follows:

$$l_{ir} \hat{\sigma}_{rs}^{trial} l_{js} = l_{ir} \hat{\sigma}_{rs}^{n+1} l_{js} + \Delta \lambda^p l_{ir} \left[ 2\bar{G} \frac{\partial F^p}{\partial \hat{\sigma}_{rs}^{n+1}} + 3(\bar{K} - \frac{2}{3}\bar{G}) \alpha_p \delta_{rs} \right] l_{js} \quad (37)$$

$$\hat{\sigma}_{ij}^{n+1} = \hat{\sigma}_{ij}^{trial} - \Delta \lambda^p \left[ 2\bar{G} \frac{\partial F^p}{\partial \hat{\sigma}_{ij}^{n+1}} + 3(\bar{K} - \frac{2}{3}\bar{G}) \alpha_p \delta_{ij} \right]$$

and from Eq. (32), the eigenvalue tensor of the plastic strain increment becomes:

$$\Delta \hat{\epsilon}_{ij}^p = \Delta \lambda^p \frac{\partial F}{\partial \hat{\sigma}_{ij}^{n+1}} \quad (38)$$

where the derivative of the potential function with respect to the principal stress tensor is given as follows:

$$\frac{\partial F^p}{\partial \hat{\sigma}_{ij}^{n+1}} = \sqrt{\frac{3}{2}} \frac{\hat{S}_{ij}^{n+1}}{\|\hat{S}_{mn}^{n+1}\|} + \alpha_p \delta_{ij} \quad (39)$$

However, using Eq. (27), one can obtain the following expression (Lee and Fenves, 2001):

$$\frac{\partial F^p}{\partial \hat{\sigma}_{ij}^{n+1}} = \sqrt{\frac{3}{2}} \frac{\hat{S}_{ij}^{trial}}{\|\hat{S}_{mn}^{trial}\|} + \alpha_p \delta_{ij} = \sqrt{\frac{3}{2}} \left[ \frac{\hat{\sigma}_{ij}^{trial} - \frac{1}{3} \bar{I}_1^{trial} \delta_{ij}}{\|\hat{S}_{mn}^{trial}\|} \right] + \alpha_p \delta_{ij} \Rightarrow$$

$$\Rightarrow = \sqrt{\frac{3}{2}} \frac{\hat{\sigma}_{ij}^{trial}}{\|\hat{S}_{mn}^{trial}\|} + \left( \alpha_p - \sqrt{\frac{1}{6}} \frac{\bar{I}_1^{trial}}{\|\hat{S}_{mn}^{trial}\|} \right) \delta_{ij} \quad (40)$$

where  $\bar{I}_1^{tr} = \hat{I}_1^{tr}$  and  $\|\bar{S}_{ij}^{tr}\| = \|\hat{S}_{ij}^{tr}\|$  are invariants ( $\|\bar{S}_{ij}^{trial}\| = \sqrt{2(\bar{J}_2)^{trial}}$ ,  $\bar{I}_1^{trial} = \bar{\sigma}_{mm}^{trial}$ ).

Now, by substituting the final form of Eq. (40) into Eq. (37) one can obtain the following form:

$$\begin{aligned}
\hat{\sigma}_{ij}^{n+1} &= \hat{\sigma}_{ij}^{trial} - \Delta\lambda^p \left[ 2\bar{G} \left( \sqrt{\frac{3}{2}} \frac{\hat{\sigma}_{ij}^{trial}}{\|\bar{S}_{mn}^{trial}\|} + \left( \alpha_p - \sqrt{\frac{1}{6}} \frac{\bar{I}_1^{trial}}{\|\bar{S}_{mn}^{trial}\|} \right) \delta_{ij} \right) + 3\left(\bar{K} - \frac{2}{3}\bar{G}\right)\alpha_p \delta_{ij} \right] \\
\hat{\sigma}_{ij}^{n+1} &= \hat{\sigma}_{ij}^{trial} - \Delta\lambda^p \left[ \sqrt{6}\bar{G} \frac{\hat{\sigma}_{ij}^{trial}}{\|\bar{S}_{mn}^{trial}\|} + 2\bar{G}\alpha_p \delta_{ij} - \sqrt{\frac{2}{3}}\bar{G} \frac{\bar{I}_1^{trial}}{\|\bar{S}_{mn}^{trial}\|} \delta_{ij} + 3\bar{K}\alpha_p \delta_{ij} - 2\bar{G}\alpha_p \delta_{ij} \right] \\
\hat{\sigma}_{ij}^{n+1} &= \hat{\sigma}_{ij}^{trial} - \Delta\lambda^p \left[ \sqrt{6}\bar{G} \frac{\hat{\sigma}_{ij}^{trial}}{\|\bar{S}_{mn}^{trial}\|} + \left( 3\bar{K}\alpha_p - \sqrt{\frac{2}{3}}\bar{G} \frac{\bar{I}_1^{trial}}{\|\bar{S}_{mn}^{trial}\|} \right) \delta_{ij} \right]
\end{aligned} \tag{41}$$

In order to obtain the expression sought out of the spectral radial-return algorithm for the maximum principal stress  $\hat{\sigma}_{max}^{n+1}$  used in the yield function, Eq. (4), one can contract the above relation such that:

$$\hat{\sigma}_{max}^{n+1} = \hat{\sigma}_{max}^{trial} - \Delta\lambda^p \left[ \sqrt{6}\bar{G} \frac{\hat{\sigma}_{max}^{trial}}{\|\bar{S}_{mn}^{trial}\|} + \left( 3\bar{K}\alpha_p - \sqrt{\frac{2}{3}}\bar{G} \frac{\bar{I}_1^{trial}}{\|\bar{S}_{mn}^{trial}\|} \right) \right] \tag{42}$$

It can be seen from Eqs. (37) and their final result, Eq. (42), that the eigenvectors are preserved throughout the corrector-steps which basically means that the effective stress eigenvectors are calculated at the predictor step and only the principal stress needs to be determined during the iterations of the plastic-corrector step (Lee and Fenves, 2001). It should also be noted that, if the eigenvalues of the plastic strain increment tensor,  $\Delta\hat{\epsilon}_{ij}^p$ , are obtained by a linear combination of  $\hat{\sigma}_{ij}^{n+1}$  and  $\delta_{ij}$ , such as for the Drucker-Prager model, Eq.(10)b, the algebraic order of the effective (undamaged) principal stresses is preserved throughout the corrector-steps. This was shown by Lee and Fenves (2001) through checking Eq. (41) and realizing that the updated effective principal stress tensor  $\hat{\sigma}_{ij}^{n+1}$  is obtained only by a scalar multiplication and constant-tensor addition/subtraction on the trial stress. Therefore, the order of the diagonal entries in the trial stress tensor cannot be changed. This argument, however, is not valid for the case where the yield criterion  $f$  given in Eq. (4) is used as a plastic potential function. This means that if one takes the derivative with respect to the maximum stresses,  $\hat{\sigma}_{max}^{n+1}$ , the algebraic order in the eigenvalue tensor does not preserve the same order.

### 2.1.3. The Effective Configuration Integration Algorithm

The radial-return mapping algorithm is derived next in order to solve for the plastic multiplier  $\Delta\lambda^p$  using the yield function discussed in Eq. (4), which can be written here at the end of the  $(n+1)$  step as:

$$\begin{aligned}
f(\bar{\sigma}_{ij}^{n+1}, (\kappa^\pm)^{n+1}) &= 0 \\
\sqrt{\frac{3}{2}} \|\bar{S}_{ij}^{n+1}\| + \alpha\bar{I}_1^{n+1} + \beta(\kappa^\pm)^{n+1} H(\hat{\sigma}_{max}^{n+1}) \hat{\sigma}_{max}^{n+1} - (1-\alpha)c^- [(\kappa^-)^{n+1}] &= 0
\end{aligned} \tag{43}$$

Applying the plasticity consistency condition given in Eq. (11) to the previous equation yields the following:

$$f^{n+1} = f^n + \frac{\partial f}{\partial \bar{\sigma}_{ij}} \Delta\bar{\sigma}_{ij} + \frac{\partial f}{\partial \hat{\sigma}_{max}} \Delta\hat{\sigma}_{max} + \frac{\partial f}{\partial \kappa^+} \Delta\kappa^+ + \frac{\partial f}{\partial \kappa^-} \Delta\kappa^- = 0 \tag{44}$$

where  $\Delta\bar{\sigma}_{ij}$  is defined here in the incremental form using Eqs. (24) and (30) as:

$$\begin{aligned}
\Delta\bar{\sigma}_{ij} &= \bar{E}_{ijkl} \Delta\bar{\epsilon}_{kl}^e = \bar{E}_{ijkl} (\Delta\bar{\epsilon}_{kl} - \Delta\bar{\epsilon}_{kl}^p) = \bar{E}_{ijkl} \Delta\bar{\epsilon}_{kl} - \bar{E}_{ijkl} \Delta\lambda^p \frac{\partial F^p}{\partial \bar{\sigma}_{kl}} \\
&= \Delta\bar{\sigma}_{ij}^{trial} - \left[ 2\bar{G}\Delta\bar{\epsilon}_{ij}^p + \left( \bar{K} - \frac{2}{3}\bar{G} \right) \Delta\bar{\epsilon}_{kk}^p \delta_{ij} \right] = \Delta\bar{\sigma}_{ij}^{trial} - \Delta\lambda^p \left[ \sqrt{6}\bar{G} \frac{\bar{S}_{ij}^{trial}}{\|\bar{S}_{mn}^{trial}\|} + 3\bar{K}\alpha_p \delta_{ij} \right]
\end{aligned} \tag{45}$$

and the principal increment  $\Delta\hat{\sigma}_{max}$  can be obtained using Eq. (42) as follows:

$$\Delta \hat{\sigma}_{\max} = \Delta \hat{\sigma}_{\max}^{trial} - \Delta \lambda^p \left[ \sqrt{6} \bar{G} \frac{\hat{\sigma}_{\max}^{trial}}{\|\bar{S}_{mn}^{trial}\|} + \left( 3\bar{K}\alpha_p - \sqrt{\frac{2}{3}} \bar{G} \frac{\bar{I}_1^{trial}}{\|\bar{S}_{mn}^{trial}\|} \right) \right] \quad (46)$$

The increments of the equivalent plastic strains  $\Delta \kappa^{\pm}$  are expressed using Eqs. (6)a,b and (38) as follows:

$$\Delta \kappa^+ = r \Delta \lambda^p \frac{\partial F^p}{\partial \hat{\sigma}_{\max}} \quad (47)$$

$$\Delta \kappa^- = -(1-r) \Delta \lambda^p \frac{\partial F^p}{\partial \hat{\sigma}_{\min}} \quad (48)$$

where  $r$  is a dimensionless parameter defined in part I of this work and in Taqueiddin (2008). Substituting Eqs. (45), (46), (47) and (48) into Eq. (44), one can obtain the following relation:

$$\begin{aligned} f^{n+1} = f^n + \frac{\partial f}{\partial \bar{\sigma}_{ij}} \left( \Delta \bar{\sigma}_{ij}^{trial} - \Delta \lambda^p \left[ \sqrt{6} \bar{G} \frac{\bar{S}_{ij}^{trial}}{\|\bar{S}_{mn}^{trial}\|} + 3\bar{K}\alpha_p \delta_{ij} \right] \right) \\ + \frac{\partial f}{\partial \hat{\sigma}_{\max}} \left( \Delta \hat{\sigma}_{\max}^{trial} - \Delta \lambda^p \left[ \sqrt{6} \bar{G} \frac{\hat{\sigma}_{\max}^{trial}}{\|\bar{S}_{mn}^{trial}\|} + \left( 3\bar{K}\alpha_p - \sqrt{\frac{2}{3}} \bar{G} \frac{\bar{I}_1^{trial}}{\|\bar{S}_{mn}^{trial}\|} \right) \right] \right) \\ + \frac{\partial f}{\partial \kappa^+} \left( r \Delta \lambda^p \frac{\partial F^p}{\partial \hat{\sigma}_{\max}} \right) + \frac{\partial f}{\partial \kappa^-} \left( -(1-r) \Delta \lambda^p \frac{\partial F^p}{\partial \hat{\sigma}_{\min}} \right) = 0 \end{aligned} \quad (49)$$

The plastic potential function derivatives,  $\frac{\partial F^p}{\partial \hat{\sigma}_{\max}}$  and  $\frac{\partial F^p}{\partial \hat{\sigma}_{\min}}$ , are given using Eq. (39) along with the Eq. (27) as functions of the trial state:

$$\frac{\partial F^p}{\partial \hat{\sigma}_{\max}} = \sqrt{\frac{3}{2}} \frac{(\hat{\sigma}_{\max}^{trial} - \frac{1}{3} \bar{I}_1^{trial})}{\|\bar{S}_{mn}^{trial}\|} + \alpha_p \quad (50)$$

$$\frac{\partial F^p}{\partial \hat{\sigma}_{\min}} = \sqrt{\frac{3}{2}} \frac{(\hat{\sigma}_{\min}^{trial} - \frac{1}{3} \bar{I}_1^{trial})}{\|\bar{S}_{mn}^{trial}\|} + \alpha_p \quad (51)$$

and the yield function derivatives,  $\frac{\partial f}{\partial \kappa^-}$  and  $\frac{\partial f}{\partial \kappa^+}$ , are obtained using Eqs. (4), (5)a,b and the definition of the variable  $\beta(\kappa^{\pm})$  (provided in part I of this work) as follows:

$$\frac{\partial f}{\partial \kappa^+} = -\frac{(1-\alpha)c^-h}{(c^+)^2} \langle \hat{\sigma}_{\max}^{n+1} \rangle \quad (52)$$

$$\begin{aligned} \frac{\partial f}{\partial \kappa^-} &= \frac{(1-\alpha)}{c^+} Q \omega \exp(-\omega \kappa^-) \langle \hat{\sigma}_{\max}^{n+1} \rangle - (1-\alpha) Q \omega \exp(-\omega \kappa^-) \\ &= (1-\alpha) Q \omega \exp(-\omega \kappa^-) \left[ \frac{\langle \hat{\sigma}_{\max}^{n+1} \rangle}{c^+} - 1 \right] \end{aligned} \quad (53)$$

Rearranging Eq. (49) to obtain an expression for  $\Delta \lambda^p$  gives the following:

$$\Delta\lambda^p = \frac{f^n + \frac{\partial f}{\partial \bar{\sigma}_{ij}} \Delta \bar{\sigma}_{ij}^{trial} + \frac{\partial f}{\partial \hat{\sigma}_{max}} \Delta \hat{\sigma}_{max}^{trial}}{H} \quad (54)$$

where

$$H = \frac{\partial f}{\partial \bar{\sigma}_{ij}} \left[ \sqrt{6G} \frac{\bar{S}_{ij}^{trial}}{\|\bar{S}_{mn}^{trial}\|} + 3\bar{K}\alpha_p \delta_{ij} \right] + \frac{\partial f}{\partial \hat{\sigma}_{max}} \left[ \sqrt{6G} \frac{\hat{\sigma}_{max}^{trial}}{\|\bar{S}_{mn}^{trial}\|} + \left( 3\bar{K}\alpha_p - \sqrt{\frac{2}{3}} \bar{G} \frac{\bar{I}_1^{trial}}{\|\bar{S}_{mn}^{trial}\|} \right) \right] - r \frac{\partial f}{\partial \kappa^+} \frac{\partial F^p}{\partial \hat{\sigma}_{max}} + (1-r) \frac{\partial f}{\partial \kappa^-} \frac{\partial F^p}{\partial \hat{\sigma}_{min}} \quad (55)$$

Note that Eq. (55) can be further simplified by realizing that:

$$\frac{\partial f}{\partial \bar{\sigma}_{ij}} = \sqrt{\frac{3}{2}} \frac{\bar{S}_{ij}^{trial}}{\|\bar{S}_{mn}^{trial}\|} + \alpha \delta_{ij} \quad (56)$$

obtained by using Eq. (27) and

$$\frac{\partial f}{\partial \hat{\sigma}_{max}} = \beta(\kappa^\pm)^{n+1} H(\hat{\sigma}_{max}^{n+1}) \quad (57)$$

where  $(\kappa^\pm)^{n+1}$  are the updated plastic variables. Applying Eqs. (56) and (57) into Eq. (55) yields the following simplified expression for  $H$ :

$$H = 3\bar{G} + 9\bar{K}\alpha_p\alpha + \beta(\kappa^\pm)^{n+1} H(\hat{\sigma}_{max}^{n+1}) \left[ \sqrt{6G} \frac{\hat{\sigma}_{max}^{trial}}{\|\bar{S}_{mn}^{trial}\|} + \left( 3\bar{K}\alpha_p - \sqrt{\frac{2}{3}} \bar{G} \frac{\bar{I}_1^{trial}}{\|\bar{S}_{mn}^{trial}\|} \right) \right] - r \frac{\partial f}{\partial \kappa^+} \frac{\partial F^p}{\partial \hat{\sigma}_{max}} + (1-r) \frac{\partial f}{\partial \kappa^-} \frac{\partial F^p}{\partial \hat{\sigma}_{min}} \quad (58)$$

It should be noted here that Eqs. (52), (53) and (57) are functions of the updated forms of the principal stress in tension  $\langle \hat{\sigma}_{max}^{n+1} \rangle$  and the plastic variables  $(\kappa^\pm)^{n+1}$ . This is the reason why local iterations are required to obtain the plastic multiplier  $\Delta\lambda^p$ . In each iteration the new evaluated trial stress will be used to update the plastic variables and the hardening functions in order to obtain an updated plastic multiplier. The process goes on until a convergence tolerance for the yield function is satisfied.

The numerator of Eq. (54) can be shown to be equal to  $f^{trial}$  during the iterative procedure by substituting Eqs. (26), (29), and (42) into Eq. (43) and considering only the terms that don not involve the plastic multiplier  $\Delta\lambda^p$  to obtain the following:

$$f^{trial} = \sqrt{\frac{3}{2}} \|\bar{S}_{ij}^{trial}\| + \alpha \bar{I}_1^{trial} + \beta(\kappa^\pm)^{trial} H(\hat{\sigma}_{max}^{trial}) \hat{\sigma}_{max}^{trial} - (1-\alpha)c^-(\kappa^-)^n \quad (59)$$

allowing Eq. (54) to be written during the iterative procedure as follows:

$$\Delta\lambda^p = \frac{f^{trial}}{H} \quad (60)$$

This concludes the elastic-plastic steps in the effective configuration. Upon convergence, the updated effective stress  $\bar{\sigma}_{ij}^{n+1}$  along with its updated elastic strain tensor  $(\bar{\epsilon}_{ij}^e)^{n+1}$  are now available to be used in the damage-corrector step in

order to update the damage variables  $(\varphi^\pm)^{n+1}$  (and therefore  $\Phi^{n+1}$ ) and the Cauchy stress tensor  $\sigma_{ij}^{n+1}$ . The flowchart shown in Figure 1 demonstrates the effective elastic-plastic integration procedure.

## 2.2. The Degradation (Damage) Step

The degradation process is termed explicit because the spectral stress ratios used in defining the damage parameter  $\Phi$  are assumed to depend on the initial stress states of each degradation increment. This is shown in Eq. (3)b, where  $\bar{\sigma}_{ij}^+$  and  $\bar{\sigma}_{ij}^-$  are the positive and negative spectral decomposition parts of the effective stress tensor,  $\bar{\sigma}_{ij}$ . This is another modification to the Tao and Phillips (2005) definition for  $\Phi$ , since their model (only elastic-damage analysis) did not include the plastic effect. Nevertheless, satisfying the damage criteria and updating the damage variables are accomplished by using the projected values (n+1) of the effective elastic strain tensor. Lee and Fenves (2001) showed that the eigenvectors of the current stress  $\sigma_{ij}^{n+1}$  are the same as those of the effective stress  $\bar{\sigma}_{ij}^{n+1}$  due to the fact that scalar degradation damage is assumed. Therefore, at the degradation corrector step, the final form of the stress tensor  $\sigma_{ij}^{n+1}$  is obtained by computing the degradation damage variable  $\Phi$ , such that:

$$\sigma_{ij}^{n+1} = (1 - \Phi) \bar{\sigma}_{ij}^{n+1} \quad (61)$$

### 2.2.1 The Damage - Corrector Step

This step starts after the effective elastic-plastic steps pass the updated forms of the effective stress tensor  $\bar{\sigma}_{ij}^{n+1}$  and its corresponding elastic strain tensor  $(\bar{\varepsilon}_{ij}^e)^{n+1}$ . The spectral decomposition of the updated effective stress tensor  $\bar{\sigma}_{ij}^{n+1}$  into positive and negative parts is then performed according to the procedure described in part I of this work and in Taqueiddin (2008). These spectral components are then used to calculate the damage release rates (damage thermodynamic conjugate forces)  $Y^\pm$  by substituting Eq. (8)c into Eq. (9) to obtain the following two equations:

$$Y^\pm = \frac{1}{2} \frac{\|(\bar{\sigma}_{ij}^\pm)^{n+1}\|}{\|(\bar{\sigma}_{ij})^{n+1}\|} \left( (\varepsilon_{ij}^e)^{n+1} \bar{E}_{ijkl} (\varepsilon_{kl}^e)^{n+1} - \frac{1}{9} \left[ \frac{1}{1 + cY^\pm \exp(-dY^\pm)} \right] ((\varepsilon_{mm}^e)^{n+1})^2 \delta_{ij} \bar{E}_{ijkl} \delta_{kl} \right) \quad (62)$$

Equations (62) ( $\pm$ ) are nonlinear functions of the conjugate forces  $Y^+$  and  $Y^-$ , respectively. Therefore, Newton-Raphson iterative procedure is used in order to solve each of these two equations independently. The procedure is demonstrated next for the thermodynamic force  $Y^i$  for expediency, where  $i$  represents (+) or (-) such that:

$$Y^i - \frac{1}{2} \frac{\|(\bar{\sigma}_{ij}^i)^{n+1}\|}{\|(\bar{\sigma}_{ij})^{n+1}\|} \left( (\varepsilon_{ij}^e)^{n+1} \bar{E}_{ijkl} (\varepsilon_{kl}^e)^{n+1} - \frac{1}{9} \left[ \frac{1}{1 + cY^i \exp(-dY^i)} \right] ((\varepsilon_{mm}^e)^{n+1})^2 \delta_{ij} \bar{E}_{ijkl} \delta_{kl} \right) = 0 \quad (63)$$

Equation (63) can be written as  $K(Y^i) = 0$  with function roots  $Y^i$  obtained using the Newton-Raphson iterative technique as follows:

$$Y_{m+1}^i = Y_m^i + \Delta Y^i = Y_m^i - K(Y_m^i) / \left( \frac{\partial K(Y^i)}{\partial Y^i} \right) \quad (64)$$

where the derivative  $\frac{\partial K(Y^i)}{\partial Y^i}$  is given as follows (evaluated at  $Y^i = Y_m^i$ ):

$$\frac{\partial K(Y^i)}{\partial Y^i} = 1 - \frac{1}{2} \frac{\|(\bar{\sigma}_{ij}^i)^{n+1}\|}{\|(\bar{\sigma}_{ij})^{n+1}\|} \left( \frac{1}{9} \left[ \frac{c \exp(-dY^i) - c d Y^i \exp(-dY^i)}{(1 + c Y^i \exp(-dY^i))^2} \right] ((\varepsilon_{mm}^e)^{n+1})^2 \delta_{ij} \bar{E}_{ijkl} \delta_{kl} \right) \quad (65)$$

Since the outcome of this iterative process is highly dependent on the “guess-value” initially suggested for  $Y_m^i = Y_0^i$ , the following form of  $Y_0^i$  was observed in this study to be convenient:

$$Y_0^i = \frac{1}{2} \frac{\|(\bar{\sigma}_{ij}^i)^{n+1}\|}{\|(\bar{\sigma}_{ij}^e)^{n+1}\|} \left( (\mathcal{E}_{ij}^e)^{n+1} \bar{E}_{ijkl} (\mathcal{E}_{kl}^e)^{n+1} \right) \quad (66)$$

The iterative procedure is terminated upon convergence of a tolerance criterion (e.g.  $\Delta Y^i \cong 0$ ).

Now that the thermodynamic conjugate forces are determined,  $Y^+$  and  $Y^-$  are substituted into Eqs. (8)a in order to check the activation of the tensile and compressive damage yield criteria  $g^+$  and  $g^-$ , respectively:

$$g^\pm = (Y^\pm)^{n+1} - Y_0^\pm - (Z^\pm)^n \leq 0 \quad (67)$$

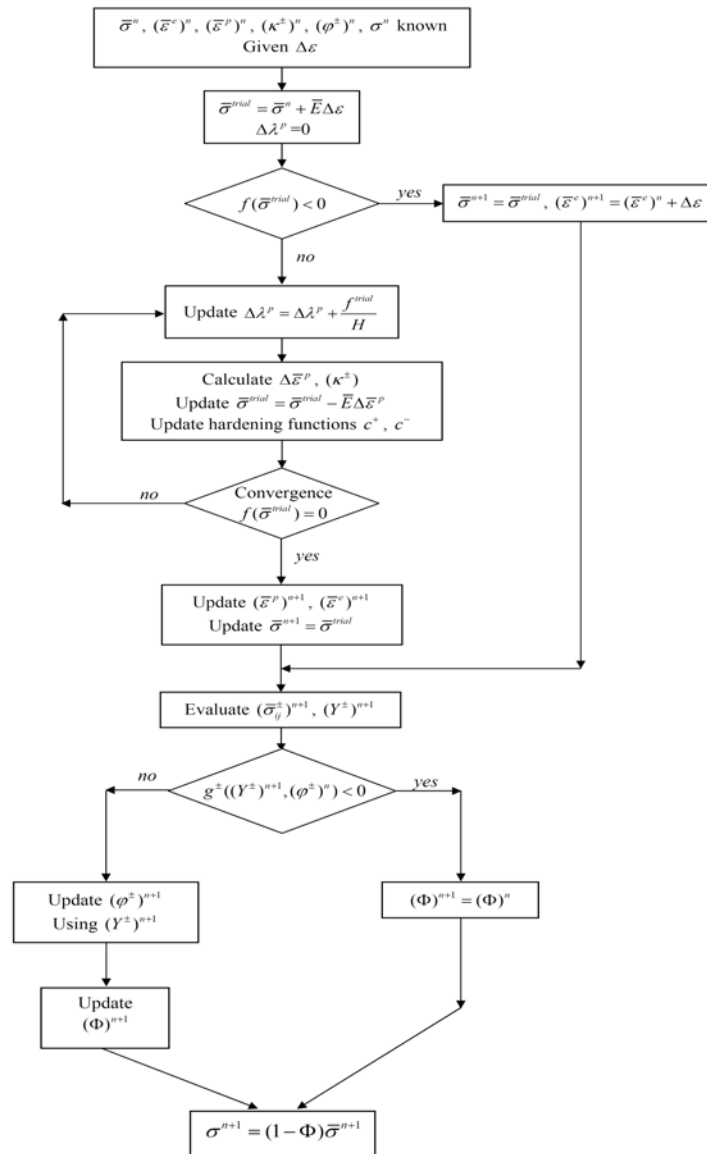


Figure 1: Integration Scheme Flowchart

If  $g^+ < 0$  and  $g^- < 0$ , the damage-corrector step ends and the Cauchy stress tensor takes the form of the updated effective stress tensor. If either of the damage criteria is activated,  $g^\pm > 0$ , damage evolution takes place and the Cauchy stress tensor is evaluation using Eq. (61). An integration algorithm is thus devised as demonstrated here to obtain the updated damage variables. These updated damage variables, along with the thermodynamic conjugate forces  $Y^+$  and  $Y^-$ , should satisfy the damage consistency conditions shown in Eq.(12), such that:

$$(Y^\pm)^{n+1} - Y_0^\pm - (Z^\pm)^{n+1} = 0 \quad (68)$$

where  $(Z^\pm)^{n+1}$  (defined in part I of this work) are given at the  $(n+1)$  step as:

$$(Z^\pm)^{n+1} = \frac{1}{a^\pm} \left( \frac{(\varphi^\pm)^{n+1}}{1 - (\varphi^\pm)^{n+1}} \right)^{\frac{1}{b^\pm}} \quad (69)$$

Substituting Eq. (69) into Eq. (68), explicit expressions for the damage variables  $(\varphi^\pm)^{n+1}$  satisfying the consistency conditions can be obtained as follows:

$$(\varphi^\pm)^{n+1} = \frac{\left( a^\pm [(Y^\pm)^{n+1} - Y_0^\pm] \right)^{b^\pm}}{1 + \left( a^\pm [(Y^\pm)^{n+1} - Y_0^\pm] \right)^{b^\pm}} = 1 - \frac{1}{1 + \left( a^\pm [(Y^\pm)^{n+1} - Y_0^\pm] \right)^{b^\pm}} \quad (70)$$

These updated damage variables can now be used to evaluate the combined scalar damage variable  $\Phi$  using Eq. (3)b. The later can then be used to update the Cauchy stress tensor as shown in Eq. (61). This concludes the damage-corrector step. Figure 1 shows an entire step of the integration scheme demonstrating the effective elastic-predictor plastic-corrector steps followed by the damage-corrector step.

### 3. Modeling of RC Beams

Considering time-independent problems, the nonlinearity of RC structures is caused by at least the following five factors (He et. al., 2006): the cracking of the concrete, the aggregate interlocking of the cracked concrete, the plasticizing and softening of the compressive concrete, bond slip between the steel and the concrete, and the dowel action of the steel reinforcement. An example of the nonlinear behavior of an RC beam in shown in Figure 2.

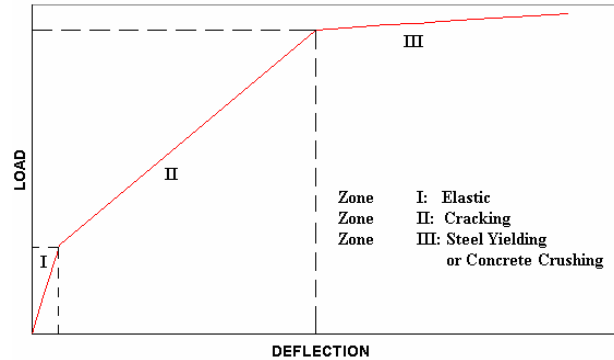


Figure 2: Typical load-displacement curve of RC beams

A constitutive model that is able to capture all of these structural nonlinearities and their microscopic as well as macroscopic effects is complex and perhaps computationally inadequate. Therefore, this is not the intended purpose of the proposed model. Because all of the above mentioned mechanisms are interacting, it is not realistic to try to formulate a constitutive model which incorporates all these mechanisms, but a model has to be formulated to adequately describe the behavior of a structure within the range of application which has been restricted in advance (Feenstra, 1993). Although the constitutive models which are developed within this phenomenological approach are usually simplified representations of the real behavior of material, it is believed that more insight can be gained by tracing the entire response of a structure in this manner, than modeling a structure with highly sophisticated material models which do not result in a converged solution after failure loads and are computationally expensive and complicated.

In order to ensure that the serviceability requirements are met in any RC structure, it is necessary to predict the cracking and the deflection of the structure under service loads. Therefore, estimation of the ultimate load is indeed essential in assessing the margin of safety of RC structures against failure. Furthermore, it is necessary to predict the load–deformation behavior of the structure for responses ranging from elastic to inelastic as well as under all possible loading conditions. Therefore, tracing the entire response of an RC structure is an essential step in the process of understanding the performance of RC, and therefore, it will be considered here.

3.1 Bond-Slip Effect on the Stress – Strain Relation of the Steel Reinforcement

Reinforcing steel is usually modeled as a linear elastic, linear strain hardening material with a yield stress  $\sigma_y$ . However, when reinforcing bars are surrounded by concrete, the average behavior of the stress–strain relation is quite different, as shown in Figure 3. Belarbi and Hsu (1994) reported that the most strikingly different feature is the lowering of the yield stress below the value of  $\sigma_y$ . Yielding of an RC member occurs when the steel stress at a cracked section reaches the yield strength of the bare bar. However, the average steel stress at a cracked element still maintains an elastic stress that is less than the yield strength, because the concrete matrix located between cracks is still partially capable of resisting tensile forces, owing to the bond between the concrete and the reinforcement.

Determination of element stiffness on the basis of the yielding of steel at a cracked section where a local stress concentration appears in the steel may result in overestimation of the structural response at the post-yielding range. Since this phenomenon is accelerated with increased deformation, an analysis of RC members subjected to loading accompanied by relatively large deformations requires the use of average stress–strain relations (Stevens et. al., 1991; Belarbi and Hsu, 1994).

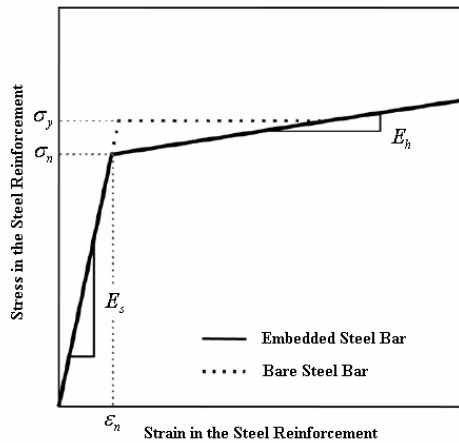


Figure 3: Stress – Strain Relation for Steel Reinforcement (Belarbi and Hsu, 1994)

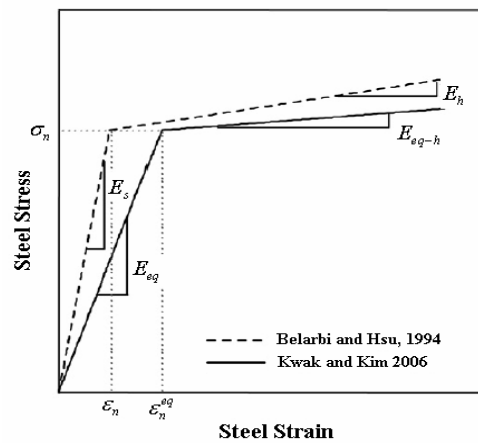


Figure 4: Stress – Strain Relation for Steel Reinforcement (Kwak and Kim, 2006)

Accordingly, the average stress–strain relation of steel needs to be defined so as to trace the cracking behavior of RC beams up to the ultimate limit state. This can be accomplished here by using continuum damage mechanics, in which the local displacement discontinuities at cracks are distributed over the finite element and where the behavior of cracked concrete is represented by the average stress–strain relations (Stevens et. al., 1991). Considering these factors, Belarbi and Hsu (1994) proposed the bilinear average stress–strain relation shown in Figure 3, which was introduced from experimental data. In Figure 3,  $\epsilon_n$  is the limiting boundary strain defined as follows:

$$\epsilon_n = \epsilon_y (0.93 - 2B) \tag{71}$$

where  $B$  is defined as  $B = (f_t' / f_y)^{1.5} / \rho_s$ ,  $f_y$  and  $\epsilon_y$  are the yield stress and the corresponding yield strain of the bare bar,  $f_t'$  is the tensile strength of concrete, and  $\rho_s$  is the steel reinforcement ratio.

Kwak and Kim (2006) elaborated on the above mentioned works and emphasized that reinforcing bars transfer tensile stresses to concrete through the bond stresses located along the surface between reinforcements and surrounding concrete. They extracted part of an RC member subjected to uniaxial tension and bounded by two adjacent cracks and used it as a free body diagram to obtain the equilibrium equations for concrete and steel using a linear bond stress-slip

relation. A reinforcing bar equivalent stress-strain relation that incorporates the effect of bond-slip is therefore developed. Their final adopted stress-strain relation for the reinforcing bars is shown in Figure 4. The equivalent elastic modulus  $E_{eq}$  is given as:

$$E_{eq} = E_s \varepsilon_{s1} / \varepsilon_{eq}^s \quad (72)$$

where  $\varepsilon_{s1}$  is the strain in the steel bar assuming perfect bond, and  $\varepsilon_{eq}^s = \int_0^{l_t} \varepsilon_s(x) dx / l_t$ . The parameter  $l_t$  represents the transfer length which can be determined following the linear relationship proposed by Somayaji and Shah (1981) on the basis of experimental data obtained from pull-out tests as follows:

$$l_t = K_p \frac{F_c}{\Sigma_o} \quad (73)$$

where  $F_c$  is the transfer load equal to  $F_c = A_c E_c \varepsilon_{s1}$ ,  $K_p$  is a constant determined from the pullout tests (Mirza and Houde, 1979), and  $\Sigma_o$  is the perimeter of a reinforcing bar. The equivalent strain  $\varepsilon_n^{ep}$  (Figure 4) is defined as  $\varepsilon_n^{ep} = \sigma_n / E_{eq}$ .

Steel reinforcement can now be included in the FE mesh as individual elements with the equivalent stress-strain relation that accounts for bond effects while assuming perfect bond between steel and concrete elements. Furthermore, the corresponding equivalent modulus of elasticity for steel  $E_{eq}$  can be used up to the yielding point in the stress-strain relation of the discrete reinforcing steel elements, as depicted by the solid line in Figure 4. The same ratio of  $E_{eq}$  to  $E_s$  given by Belarbi and Hsu (1994) was assumed by Kwak and Kim (2006) to be maintained at the post-yielding region.

### 3.2 Applications of the Constitutive Model to the FE Analysis of RC Beams

The proposed model is applied first to study the simply supported RC beam tested experimentally by Burns and Siess (1962) and later modeled by Kwak and Filippou (1997). The tested specimen consisted of a simply supported beam with a span of 12 ft (3.7 m) which was subjected to a concentrated load at midspan. The geometry and the cross section of the beam are shown in Figure 5 and the material properties are given as follows: The moduli of elasticity for concrete and steel are  $E_c = 3800$  Ksi and  $E_s = 29500$  Ksi, respectively. The tensile and compressive strengths of concrete are  $f_o^+ = 0.347$  Ksi and  $f_c^- = 4.82$  Ksi, respectively. The yielding stress for the steel bars is  $f_y = 44.9$  Ksi. The reinforcement consists of #6 (0.75 in diameter) rebars with a reinforcement ratio of  $\rho_s = 0.99\%$ . The reinforcement is modeled using 2 dimensional elements (Figure 6). The constitutive model of these elements accounts for the bond effect as described in section (3.1). The Poisson's ratios for concrete and steel are  $\nu_c = 0.167$  and  $\nu_s = 0.333$ , respectively. The fracture energy is given as  $G_f = 0.5$  lb/in.

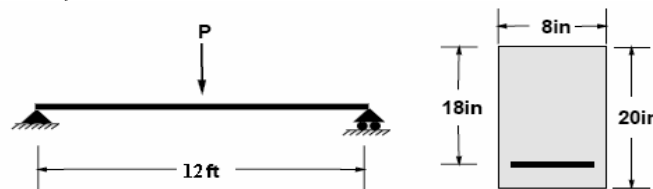


Figure 5: Geometry and cross section of RC beam (Burns and Siess, 1962)

Only half of the beam is modeled in this FE simulation by taking advantage of the symmetry in the geometry and loading. The FE discretization, the arrangement of the steel reinforcement, and the loading and support conditions are shown in the Figure 6.

Three analyses were carried out using four-nodded quadrilateral elements and 100 deflection/time increments. The same model parameters used for the concrete beam analysis in part I of this work are used here. The fracture energy, along with the characteristic lengths for different meshes provided by ABAQUS, is used to reduce the effect of mesh sensitivity. Figures 7, 8, and 9 show the results of the tensile damage variable  $\phi^+$  at the end of the FE incremental procedures involving three different mesh sizes, 78, 156, and 312 elements. Figures 10, 11, and 12 shows idealized

tensile damage distributions - plotted over undeformed meshes - that are used to compare results to each other (Figure 13) as well as to the damage distribution obtained by Kwak and Filippou (1997) as shown in Figure 14.

The load-deflection curves obtained using the three simulations discussed above are shown in Figure 15. The results are compared to the experimental output of the work of Burns and Siess (1962). It can be seen that the numerical results exhibit fluctuations that are related to convergence issues, especially in the zone where concrete is softening under compression (crushing of concrete). The compressive damage material parameters are the ones that govern the shape of the load-deflection curves beyond the 30 Ksi stress level. The mesh sensitivity is reduced by using the fracture energy related coefficient  $\gamma^-$ .

Figures 16, 17, and 18 show the total damage ( $\Phi$ ) distributions for the three simulations discussed above. The total damage variable  $\Phi$  (scalar) is obtained using Eq. (3)b. It should be noted here that the total damage variable is a weighted average function of the stress tensor as well as its spectral decomposition parts, and the tensile  $\varphi^+$  and compressive  $\varphi^-$  scalar damage variables. This averaging technique results in the differences between the tensile damage distributions and the total damage distributions plotted in the previously indicated figures.

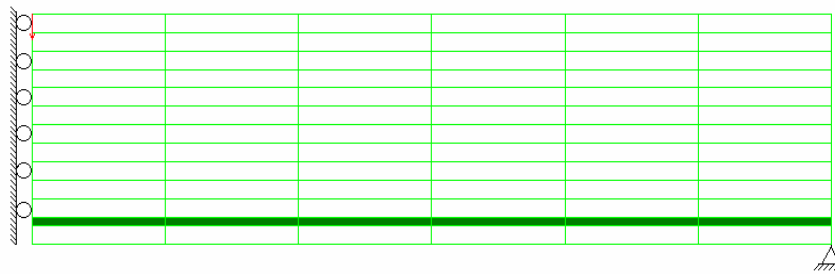


Figure 6: FE discretization of steel and concrete, loading, and support conditions

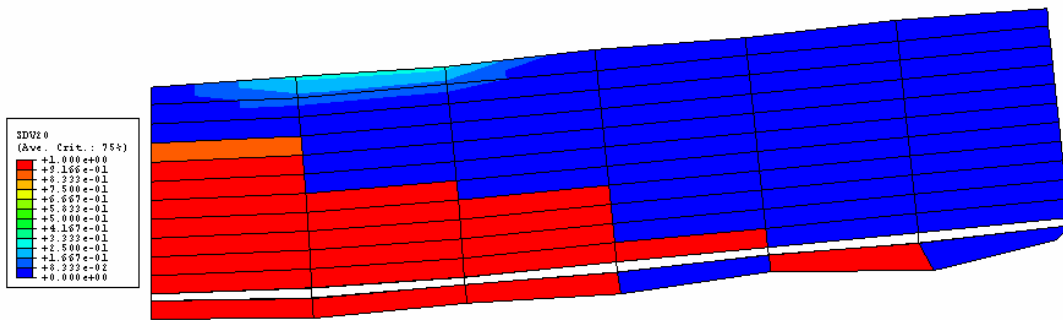


Figure 7: Tensile damage  $\varphi^+$ , coarse mesh 78 elements

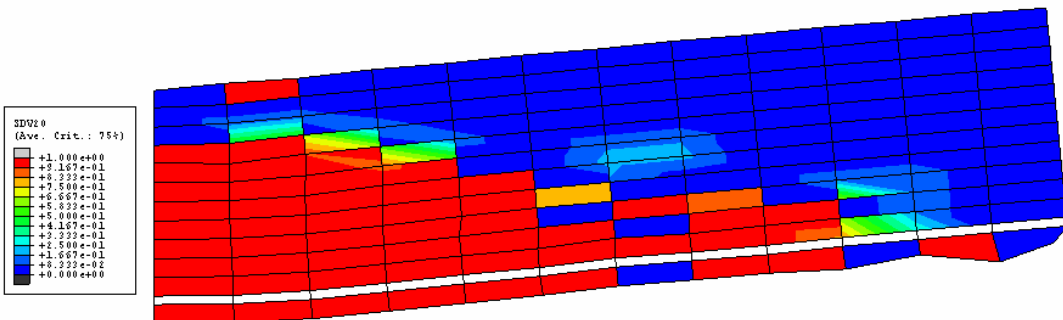


Figure 8: Tensile damage  $\varphi^+$ , finer mesh 156 elements



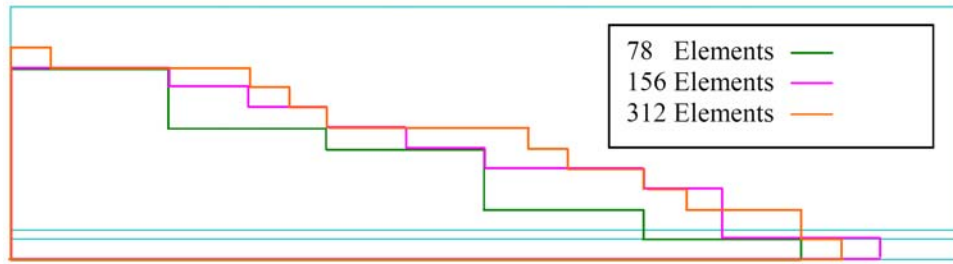


Figure 13: Idealized tensile damage distributions



Figure 14: Damage distribution, results obtained by Kwak and Filippou (1997)

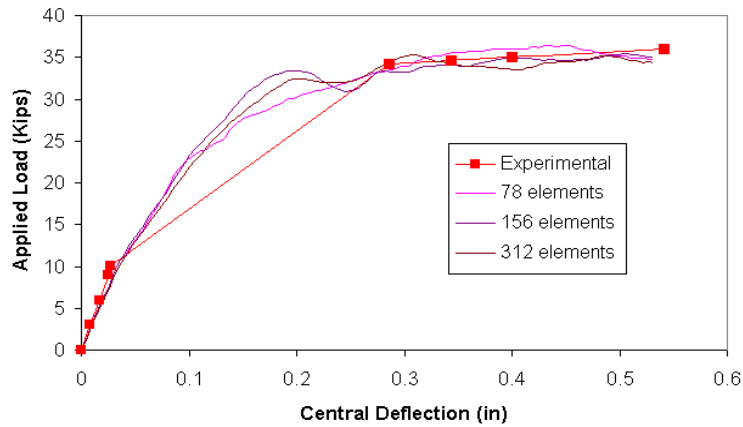


Figure 15: Load-Deflection relations for RC beam (Burns and Siess, 1962)

The proposed model is also applied to study the simply supported RC beams tested experimentally by Karihaloo (1992) and later modeled by Tikhomirov and Stein (2001). Three point bending of the experimental RC specimens was carried out. Two beams with one and two 12 mm diameter bars are analyzed until failure occurred in a displacement controlled environment. The geometry and the cross sections of the beams are shown in Figures. 19 and 25. The material properties used are as follows: The moduli of elasticity for concrete and steel are  $E_c = 30$  GPa and  $E_s = 200$  GPa, respectively. The tensile strength of concrete is  $f_o^+ = 2.26$  MPa. The yielding stress for the steel bars is  $f_y = 463$  MPa. The reinforcement is again modeled using 2 dimensional elements. The constitutive model of these elements did not account for the bond effect, since the results underestimate the RC beam strength, see Figures. 24 and 26. The Poisson's ratios for concrete and steel are  $\nu_c = 0.2$  and  $\nu_s = 0.3$ , respectively.

Only half of each beam is modeled in these FE simulations by taking advantage of the symmetry in the geometry and loading conditions. The first analysis was performed using a 360 element mesh with 45 elements representing the steel reinforcement as can be seen in Figure 20. The damage distributions are similar in pattern to those of the previous example. The averaging of the properties used in obtaining the total damage  $\Phi$  distribution is again the reason for the differences between the tensile  $\phi^+$  and total damage  $\Phi$  distributions (see Figures 20 and 21).

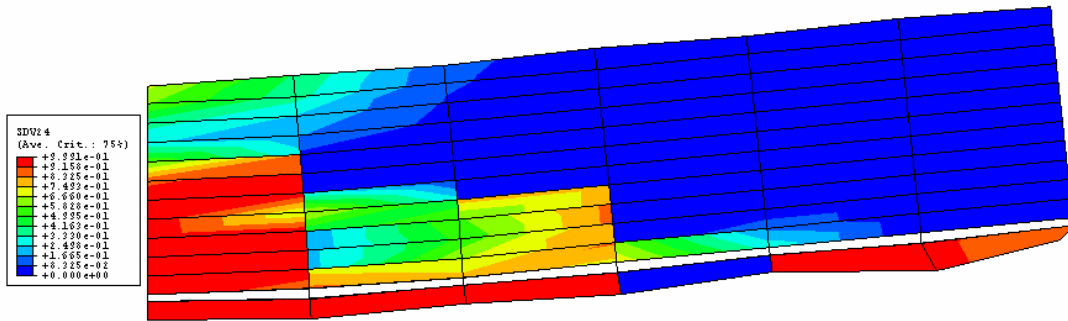


Figure 16: Total damage  $\Phi$  , coarse mesh 78 elements

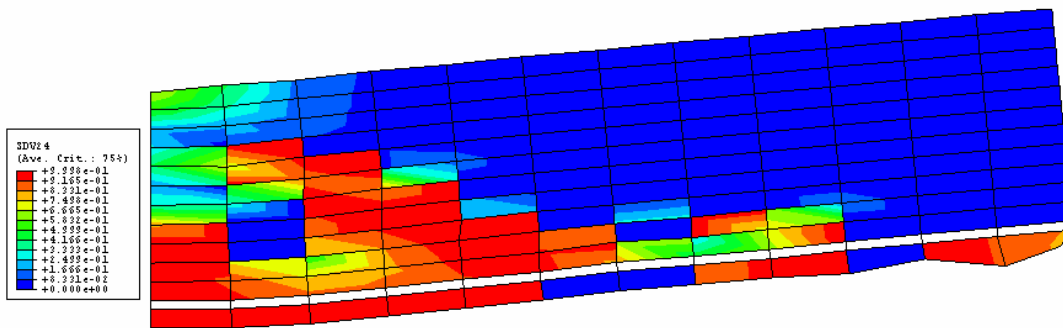


Figure 17: Total damage  $\Phi$  , finer mesh 156 elements

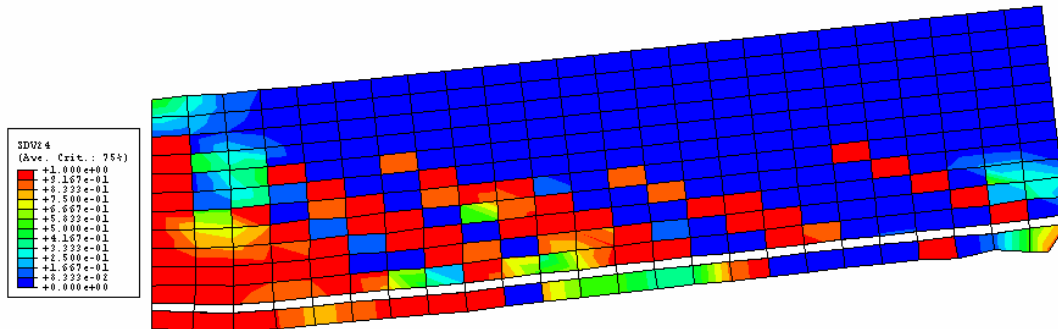


Figure18: Total damage  $\Phi$  , finer mesh 312 elements

In Figure 22, damage is plotted over the undeformed mesh in order to compare the proposed model's damage distribution to that of Tikhomirov and Stein (2001), Figure 23. The load-deflection curves obtained using the FE simulation discussed above is shown in Figure 24. The results are compared to the experimental output of the work of Karihaloo (1992). The numerical results exhibit fluctuations similar to those in Figure 15, and are again believed to be related to convergence issues. The model's behavior underestimates the strength of the RC beam in the intermediate stage where concrete is deteriorating. This was not observed in the previous example, where all three simulations showed overestimation of the strength in the same region. Nevertheless, the trend of the results is close to the experimental ones demonstrating the ability of the proposed model's to capture the physical behavior of RC.

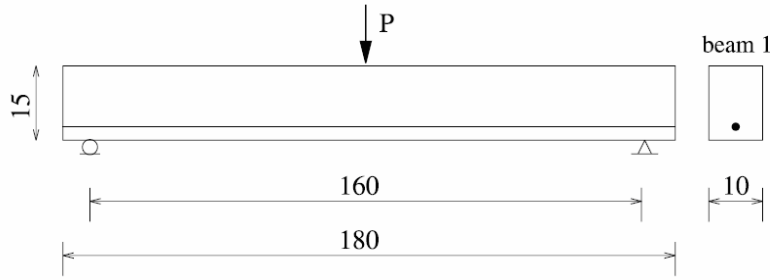


Figure19: Geometry and cross section of RC beam 1 (Karihaloo, 1992)

Figure 26 shows the load-deflection curves obtained using the FE simulation of the second beam with two 12mm reinforcing bars. The same number of elements used in the previous example is adopted here. The simulated results are again compared to the experimental output of the work of Karihaloo (1992). The experimental results show a more brittle failure of the RC beam when compared to the previous one (one 12mm bar) where the beam fails through yielding of steel. This is a direct result of increasing the amount of reinforcement (2 bars). The numerical behavior, on the other hand, underestimates the strength of the RC beam in the intermediate stage where concrete is deteriorating. The trend of the results is close to the experimental ones, demonstrating again the ability of the proposed model's to capture the physical behavior of RC.

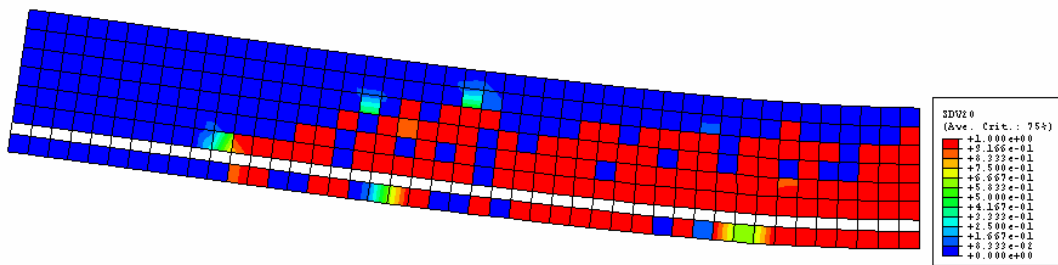


Figure 20: Tensile Damage  $\varphi^+$  distribution, 360 elements mesh

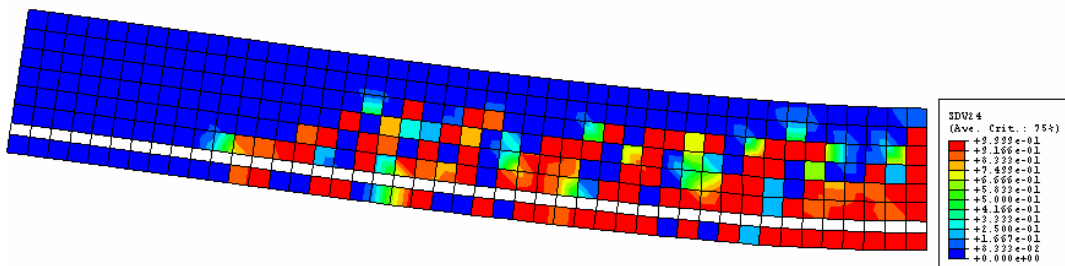


Figure 21: Total Damage  $\Phi$  distribution, 360 elements mesh

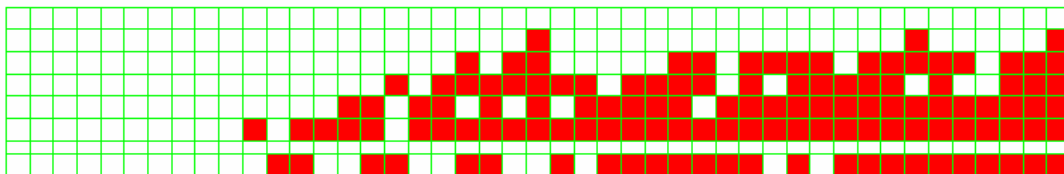


Figure 22: Idealized Tensile damage distribution

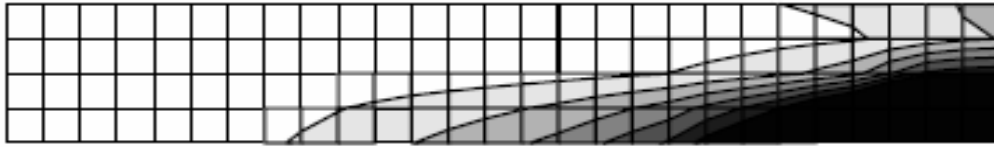


Figure 23: Damage distribution obtained by Tikhomirov and Stein (2001)

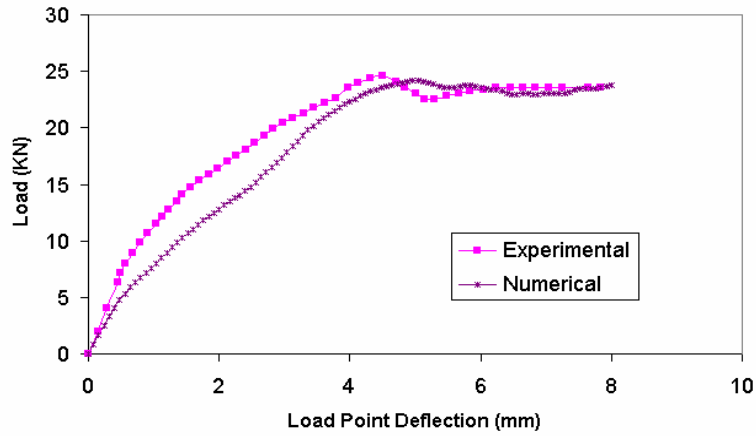


Figure 24: Load-central deflection relation for RC beam 1 (Karihaloo, 1992)

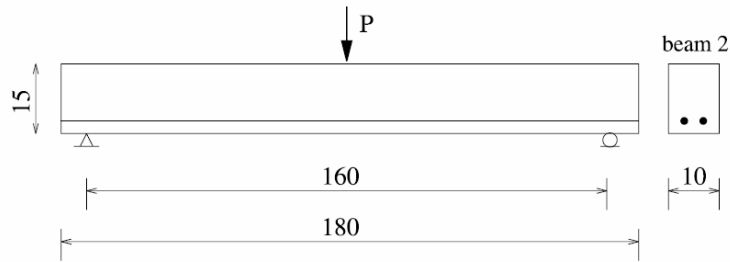


Figure 25: Geometry and cross section of RC beam 2 (Karihaloo, 1992)

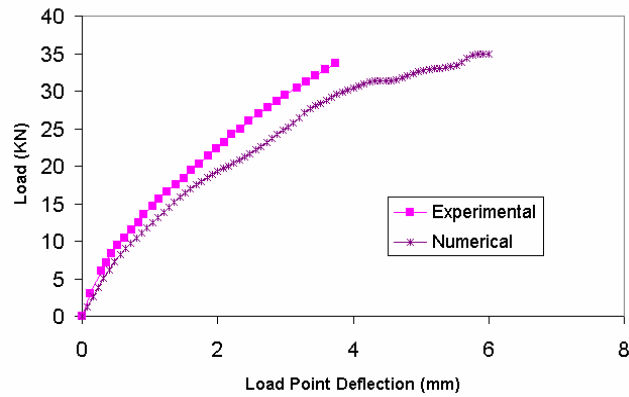


Figure 26: Load-central deflection relation for RC beam 2 (Karihaloo, 1992)

#### 4. Conclusions

The computational algorithm for the numerical integration of the concrete constitutive model described in part I of this work is discussed and presented in details. Based on the operator split concept, the incremental constitutive equation is decomposed into elastic, plastic and damage parts, leading to the corresponding numerical elastic-predictor, plastic-corrector and damage-corrector steps. During the first two steps, the damage variables are fixed, so that the elastic-plastic behavior is decoupled from damage, constituting a standard elastic-plastic problem in the effective stress space. The damage variables and the Cauchy stress tensor can then be updated correspondingly in the damage-corrector step. An elastic-plastic implicit, damage explicit integration scheme is adopted here to address both concrete and reinforced concrete. The consistent elastic-plastic-damage tangent operator is derived in part I of this work and a flow chart of the integration technique is provided here for completeness.

In order to analyze the reinforced concrete "RC" beams, the bond-slip effect along the reinforcing bars is quantified with the force equilibrium and compatibility condition at the post-cracking stage. This effect is indirectly implemented into the stress-strain relation of reinforcing steel. The advantage of such procedure is taking into account the incorporation of the bond slip effect while using the conventional discrete representation of steel, without the need for additional considerations such as using double nodes, interface elements, or modified finite element formulation to produce more complicated element library. This approach is more suited to the material modeling using the UMAT subroutine, where all the numerical procedures are written in terms of stresses and strains.

The macroscopic components of RC members are modeled using separate constitutive models. Elastoplastic constitutive models with strain hardening are used to model the behavior of steel reinforcement, and a continuum approach based on damage mechanics and plasticity theory is adopted to describe the complex behavior of concrete material in structural elements. The concept of energy dissipation (fraction energy) is used in order to reduce the effect of mesh sensitivity on the FE numerical results. Bond and interaction between steel and concrete is accounted for by modifying the global stress-strain curve of steel reinforcement to account for the reduction in the strength (elastic and plastic moduli and yield stress) observed experimentally. All these components are integrated into the proposed approach in an attempt to properly describe the complex physical behavior of RC composite materials.

The implemented algorithms are then used to analyze two simply supported RC beams subjected to concentrated loads applied at mid spans. The proposed model is able to capture the three stages of loading shown in Figure 2. An attempt to reduce the variation in the numerical results is carried out by means of adjusting the fracture energy related parameters. As the mesh size is reduced, the results varied yet remained close to one another, a behavior attributed to a non regularized constitutive approach.

In conclusion, the proposed approach of analysis of concrete and RC beams is a meaningful experience. It spots the light on many issues relating to the constitutive modeling of RC; one of the most challenging fields in Civil Engineering. Despite all the research done in the past, a current literature review shows that scientists still believe in the potential for further improvement of the way RC materials are studied and designed. This particular study reveals more questions than answers; allowing endless space for future development.

#### References

- Belarbi, A. and Hsu, T. C. (1994). Constitutive laws of concrete in tension and reinforcing bars stiffened by concrete, *ACI Structural Journal* **91(4)**, pp. 465–74.
- Burns, N.H. and Siess, C.P. (1962). Load-Deformation Characteristics of Beam-Column Connections in Reinforced Concrete, *Civil Engineering Studies* SRS No. **234**, University of Illinois, Urbana.
- Červenka, J. and Papanikolaou, V. K. (2008). Three dimensional combined fracture-plastic material model for concrete, *Int. J. Plasticity*, Available online 5 February, in press.
- Cicekli, U., Voyiadjis, G. Z. and Abu Al-Rub, R. K. (2007). A plasticity and anisotropic damage model for plain concrete, *Int. J. Plasticity* **23(10-11)**, pp. 1874-1900.
- Contrafatto, L. and Cuomo, M. (2006). A framework of elastic-plastic damaging model for concrete under multiaxial stress states, *Int. J. Plasticity* **22(12)**, pp. 2272-2300.
- Faria, R., Oliver, J. and Cervera, M. (1998). A strain-based plastic viscous-damage model for massive concrete structures, *Int. J. Solids and Struct.* **35(14)**, pp. 1533-1558.
- Feenstra, P. H. (1993). Computational aspects of biaxial stress in plain and reinforced concrete, Dissertation, *Delft University*, the Netherlands.
- Fichant, S., La Borderie, C. and Pijaudier-Cabot, G. (1999). Isotropic and anisotropic descriptions of damage in concrete structures, *Int. J. Mech. Cohesive Frictional Mater.* **4**, pp. 339–359.
- He, W., Wu, Y. F., Liewand, K. M. and Wu, Z. (2006). A 2D total strain based constitutive model for predicting the behaviors of concrete structures, *Int. J. of Eng. Science* **44(18-19)**, pp. 1280-1303.

- Jason, L., Huerta, A., Pijaudier-Cabot, G. and Ghavamian, S. (2006). An elastic plastic damage formulation for concrete: Application to elementary tests and comparison with an isotropic damage model, *Comp. Meth. in Applied Mech. and Eng.* **195(52)**, 7077-7092.
- Jefferson, A. D. (2003). Craft—a plastic damage contact model for concrete - I. Model theory and thermodynamic considerations, *Int. J. Solids Struct.* **40**, pp. 5973-5999.
- Ju, J. W. (1989). On energy-based coupled elasto-plastic damage theories: constitutive modeling and computational aspects, *Int. J. Solids and Struct.* **25(7)**, 803-833.
- Lee, J. and Fenves, G. L. (1998). A plastic-damage model for cyclic loading of concrete structures, *J. Eng. Mech., ASCE* **124**, pp. 892-900.
- Lee, J. and Fenves, G. L. (2001). A return-mapping algorithm for plastic-damage models: 3-D and plane stress formulation, *Int. J. Num. Meth. Eng.* **50**, pp. 487-506.
- Karihaloo B. L. (1992). Failure modes of longitudinally reinforced beams. In Carpinteri, A., editor. Application of fracture mechanics to reinforced concrete. London: Elsevier, pp. 523-546.
- Kwak, H. G. and Filippou F. C. (1997). Nonlinear FE Analysis of R/C Structures Under Monotonic Loads, *Computers & Structures* **65(1)**, pp. 1-16.
- Kwak, H. G. and Kim, J. K. (2006). Implementation of bond-slip effect in analyses of RC frames under cyclic loads using layered section method, *J. Eng. and Struct.* **28**, 1715-1727.
- Mazars, J. and Pijaudier-Cabot, G. (1989). Continuum damage theory - application to concrete, *J. Eng. Mech.* **115(2)**, pp. 345-365.
- Mirza, S. M. and Houde, J. (1979). Study of bond stress–slip relationships in reinforced concrete, *ACI J.* **76(1)**, pp. 19–45.
- Nechnech, W., Meftah, F. and Reynouard, J. M. (2002). An elasto-plastic damage model for plain concrete subjected to high temperatures, *J. of Eng. Struct.* **24(5)**, pp. 597-611.
- Salari, M. R., Saeb, S., Willam, K. J., Panchet, S. J. and Carrasco, R. C. (2004). A coupled elastoplastic damage model for geomaterials, *Comp. Meth. in Applied Mech. and Eng.* **193(27-29)**, 2625-2643.
- Shen, X., Yang, L. and Zhu, F. (2004). A Plasticity-based Damage Model for Concrete, *Adv. in Struct. Eng.* **7(5)**, pp. 461-467.
- Simo, J.C. (1992). Algorithm for static and dynamics multiplicative plasticity that preserve the classical return mapping schemes of the infinitesimal theory, *Comp. Meth. Appl. Mech. Eng.* **99**, pp. 61-112.
- Simo, J. and Hughes, T. (1998). Computational inelasticity, *Springer-Verlag*, New York.
- Somayaji, S. and Shah, S. P. (1981). Bond stress versus slip relationship and cracking response of tension members, *ACI J.* **78(3)**, pp. 217–25.
- Stevens, N. J., Uzumeri, S. M., Collins, M. P. and Will, G. T. (1991). Constitutive model for reinforced concrete finite element analysis, *ACI Struct. J.* **88(1)**, pp. 49-59.
- Tao, X. and Phillips, D. V. (2005). A simplified isotropic damage model for concrete under bi-axial stress states, *Cement and Concrete Composites* **27(6)**, pp.716-726.
- Taqueiddin, Z. N. (2008). Elasto-Plastic and Damage Modeling of Reinforced Concrete. Dissertation, *Louisiana State University*, Louisiana, USA.
- Tashman, L., Masad, E., Little, D. and Zbib, H. (2005). A microstructure-based viscoplastic model for asphalt concrete, *Int. J. Plasticity* **21(9)**, pp. 1659-1685.
- Tikhomirov, D. and Stein, E. (2001). Finite element computations of anisotropic continuum damage in reinforced concrete, *Computers & Structures* **79(22-25)**, pp. 2249-2260.
- Voyiadjis, G. Z. and Taqueiddin, Z. N. (2008). Elastic Plastic and Damage Model for Concrete Materials. Part I: Theoretical Formulation, *Int. J. Plasticity*, submitted for publication.
- Voyiadjis, G. Z., Taqueiddin, Z. N. and Kattan, P. I. (2008a). Theoretical Formulation of a Coupled Elastic-Plastic Anisotropic Damage Model for Concrete using the Strain Energy Equivalence Concept, *Int. J. of Damage Mech.*, in press.
- Voyiadjis, G. Z., Taqueiddin, Z. N. and Kattan, P. I. (2008b). Anisotropic Damage-Plasticity Model for Concrete, *Int. J. Plasticity*, available online, in press.
- Willam, K., Rhee, I. and Xi, Y. (2003). Thermal degradation of heterogeneous concrete materials. Special issue on Durability, *J. Mat. Civil Eng. ASCE* **17(3)**, pp. 276-285.
- Wu, J. Y., Li, J. and Faria, R. (2006). An energy release rate-based plastic-damage model for concrete, *Int. J. of Solids and Struct.* **43(3-4)**, pp. 583–612.
- Yazdani, S. and Schreyer, H. L. (1990). Combined plasticity and damage mechanics model for plain concrete, *J. Eng. Mech. ASCE* **116(7)**, pp. 1435-1450.